CHAPTER V

RESULTS AND DISCUSSION

The results and discussion in this chapter are divided into three sections. Section 5.1 is described the influence of concentration of aluminum isopropoxide in 1-butanol used in the preparation of nanocrystalline alumina by solvothermal method on the properties of alumina powders and alumina supported-cobalt catalysts. Section 5.2 explains the effect of mixed γ and χ crystalline phases in Al_2O_3 on the characteristics and catalytic activities of alumina-supported cobalt catalysts. The effect of Cu as an Al_2O_3-modifier on the characteristics and catalytic activities of alumina-supported iron catalysts during FTS reaction are illustrated in section 5.3.

5.1 The influence of concentration of aluminum isopropoxide in 1-butanol used in the preparation of nanocrystalline alumina by solvothermal method on the properties of alumina powders and alumina supported-cobalt catalysts during CO hydrogenation reaction

5.1.1 Effect of AIP concentration on the properties of Al_2O_3

5.1.1.1 X-ray diffraction (XRD)

Figure 5.1 shows the XRD patterns of various alumina powders obtained from thermal decomposition of AIP in 1-butanol after calcination at 600°C for 1 h. XRD patterns of Al_2O_3 show strong diffraction peaks at 31°, 33°, 38°, 43°, 47.5°, and 68° (according to the JCPDSs database). It was found that when lower amounts of AIP were used, only γ-alumina was formed as seen by the XRD characteristic peaks at 2θ = 33° according to the JCPDSs database. The XRD characteristic peaks of χ-alumina was observed at 2θ = 42.5° for the ones prepared with AIP 25 and 35 g. The intensity of χ-alumina peaks became stronger with increasing amount of AIP content. It is indicated that increasing AIP content during the synthesis resulted in formation of mixed phase between γ-alumina and χ-alumina.

The crystallization process of alumina was probably affected by the amounts of AIP in 1-butanol.

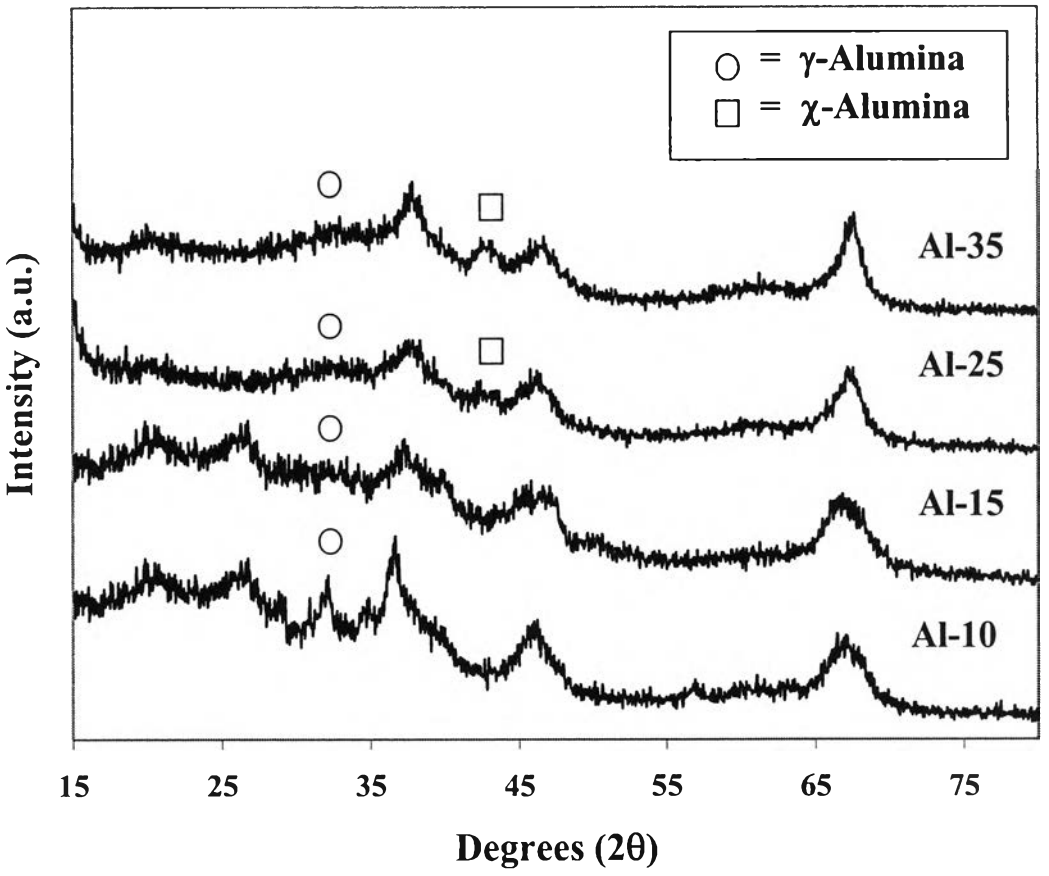

Figure 5.1 XRD patterns of various nanocrystalline alumina prepared by the reaction of AIP in 1-butanol at 300°C for 2 h (after calcinations at 600°C for 1 h).

5.1.1.2 Transmission Electron Microscopy (TEM)

TEM images of alumina powders prepared with different amounts of AIP are shown in Figure 5.2. For the ones prepared with lower amounts of AIP, Al-10 and Al-15, the wrinkled sheets morphology was observed. They were found to be similar to those obtained from the formation of γ-alumina by decomposition of glycol or alkyl derivatives on boehmite (Inoue *et al.*, 1996c; Praserthdam *et al.*, 2000). As the amounts of AIP increased, the wrinkled sheets morphology became less apparent and spherical particles were observed. The presence of spherical particles were probably due to the formation of χ-alumina, which was normally formed by thermal decomposition reaction of AIP in inert organic solvents at 300°C (Mekasuwandumrong *et al.*, 2004a; Mekasuwandumrong *et al.*, 2004b; Mekasuwandumrong *et al.*, 2003; Praserthdam *et al.*, 2000). TEM results were in a good agreement with the XRD patterns that the mixture of γ-alumina and χ-alumina was observed when AIP concentration increased.

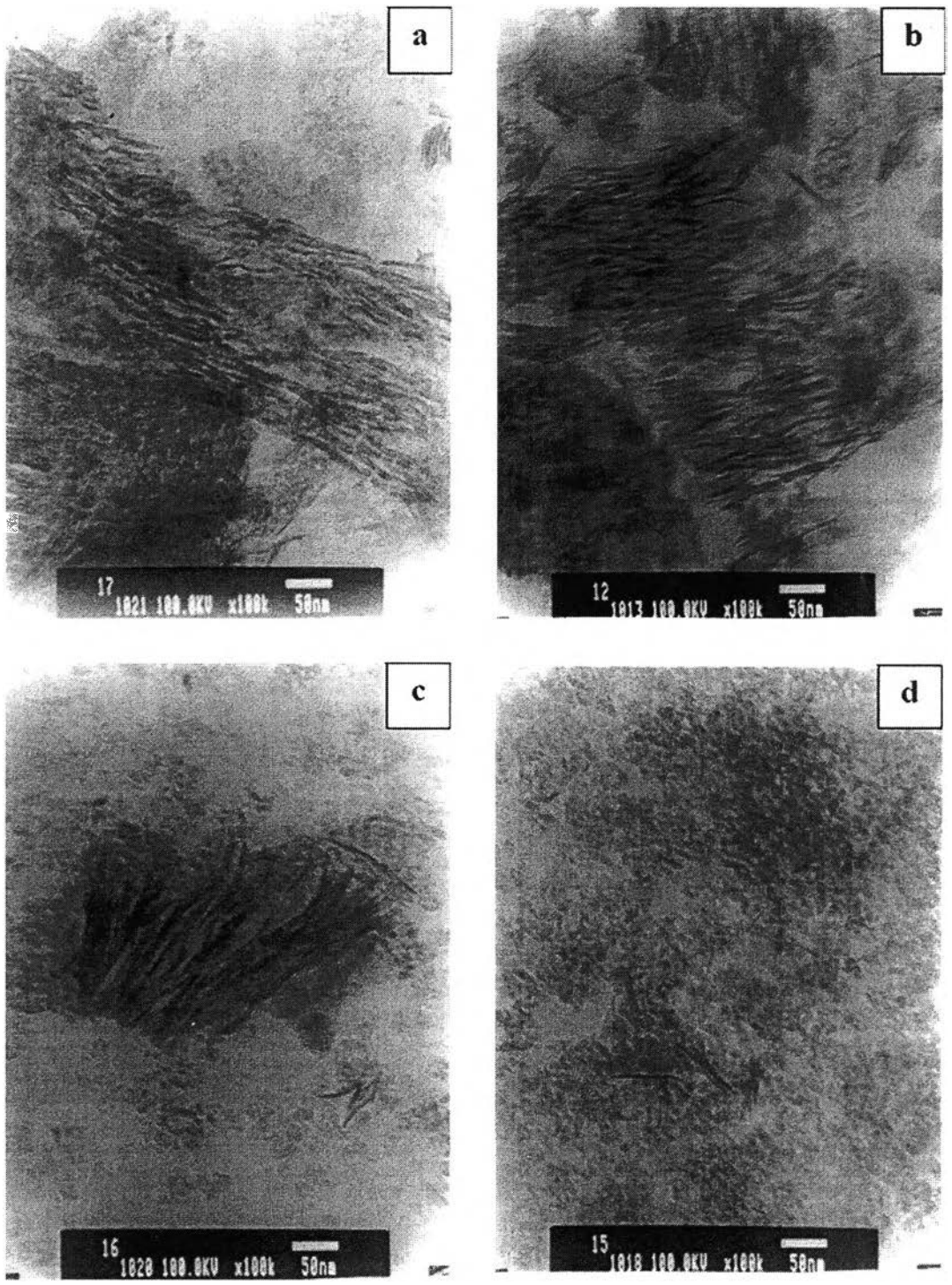

Figure 5.2 TEM images of alumina obtained by the reaction of AIP in 1-butanol at 300°C for 2 h with different amounts of AIP (a) Al-10 (b) Al-15 (c) Al-25 (d) Al-35.

5.1.1.3 Bulk density and BET surface area

The physical properties of the alumina products are summarized in Table 5.1. The BET surface areas increased with increasing AIP concentration as a result of morphology changing from wrinkled sheets structure to small spherical particles. BET surface area of the Al-35 (145 m^2/g) was found to be twice of that of Al-10 (70 m^2/g). Similar trend was observed for the bulk density of the alumina powders. The bulk density increased with increasing AIP contents.

Table 5.1 The physical and chemical properties of Al_2O_3 supports.

Samples	Amounts of AIP (g)	Surface area $(m^2/g)^a$	Bulk density $(g/cm^3)^a$	Morphology
Al-10	10	70	0.3824	Wrinkled sheets
Al-15	15	120	0.3858	High amount of wrinkled sheets
Al-25	25	139	0.3928	Wrinkled sheets and small amount of spherical particles
Al-35	35	145	0.5358	Small amount of wrinkled sheets and high amount of spherical particles

[a] Error of measurement = ± 5%.

Mechanism of thermal decomposition of AIP in alcohol has been proposed in our previous works (Mekasuwandumrong *et al.,* 2004a; Praserthdam *et al.,* 2000) involving three competitive reactions. First, AIP reacted with 1-butanol yielding aluminum butoxide, which decomposed further to give the alkyl (butyl) derivative of boehmite. Second, 1-butanol can be dehydrated to give water which then hydrolyzes aluminum isopropoxide or butoxide yielding pseudoboehmite. Finally, the direct decomposition of aluminum alkoxide in organic solvent, which proceeded slowest, gave χ-alumina. In the present works, at low AIP contents, boehmite was probably the main product and γ-alumina was obtained after calcination at 600°C for 1 h. The morphology of the boehmite products obtained via solvothermal reaction was wrinkled sheets (Mekasuwandumrong *et al.,* 2004a; Praserthdam *et al.,* 2000), which was also similar to those of γ-alumina decomposed from. However, when the amounts of AIP in 1-butanol increased, formation of χ-alumina from direct decomposition of AIP in the solvent occurred as the main reaction.

5.1.2 Characteristics of 10% Co/Al_2O_3 catalysts

5.1.2.1 X-ray diffraction (XRD)

The XRD patterns of cobalt catalysts supported on alumina prepared with various amounts of AIP are shown in Figure 5.3. The XRD patterns of the Co/Al_2O_3 catalysts were not significantly different from those of alumina supports. No XRD peaks of Co_3O_4 or other Co compounds were detected. This indicates that cobalt was present in a highly dispersed form on alumina even for cobalt loading as high as 10 wt% (Jongsomjit *et al.*, 2003).

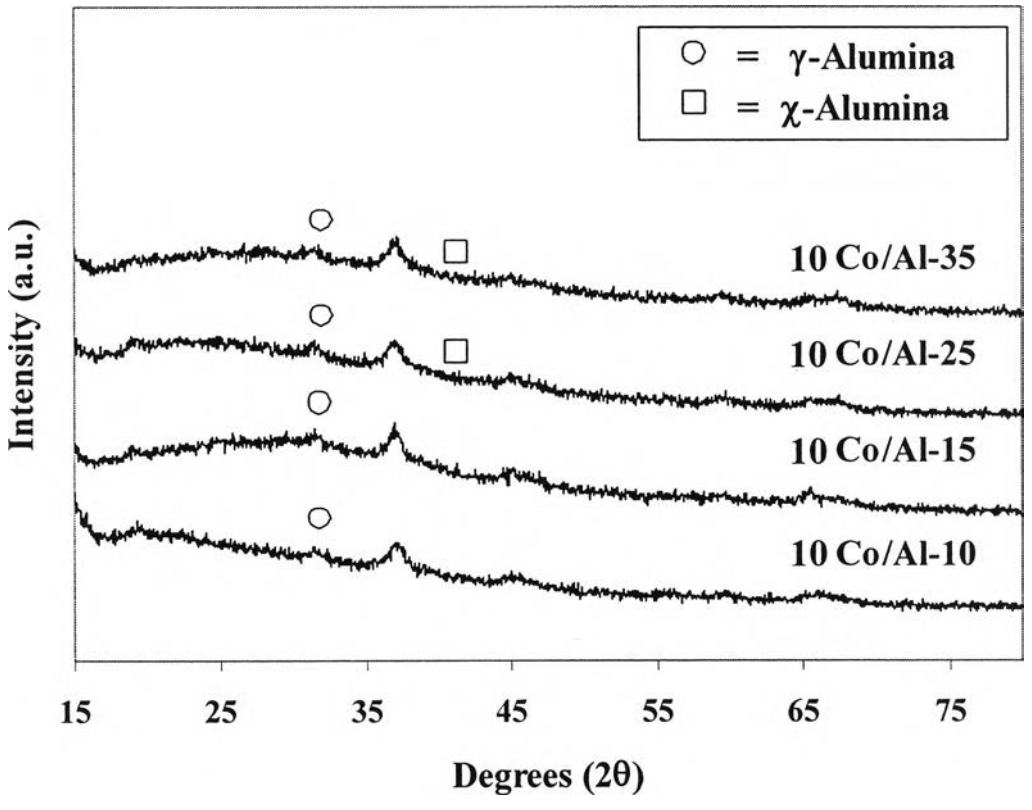

Figure 5.3 XRD patterns of 10% Co/Al_2O_3 catalysts with different amounts of AIP.

5.1.2.2 Electron microscopy

SEM and EDX were performed in order to study the morphology and elememtal distribution of the catalyst samples, respectively. Typical SEM micrographs of 10% Co/Al_2O_3 catalysts are shown in Figure 5.4. There was no significant change in morphology of the catalyst samples due to the effect of AIP concentrations in 1-butanol used in the preparation process. The white or light spots observed in all figures can be attributed to the cobalt patches distributed on the external surface of catalyst granules. Figure 5.5 shows the SEM micrographs and the EDX mapping of the cross-sectioned 10Co/Al-35 catalyst granule. The distribution of cobalt was found to be well dispersed through out the catalyst granule.

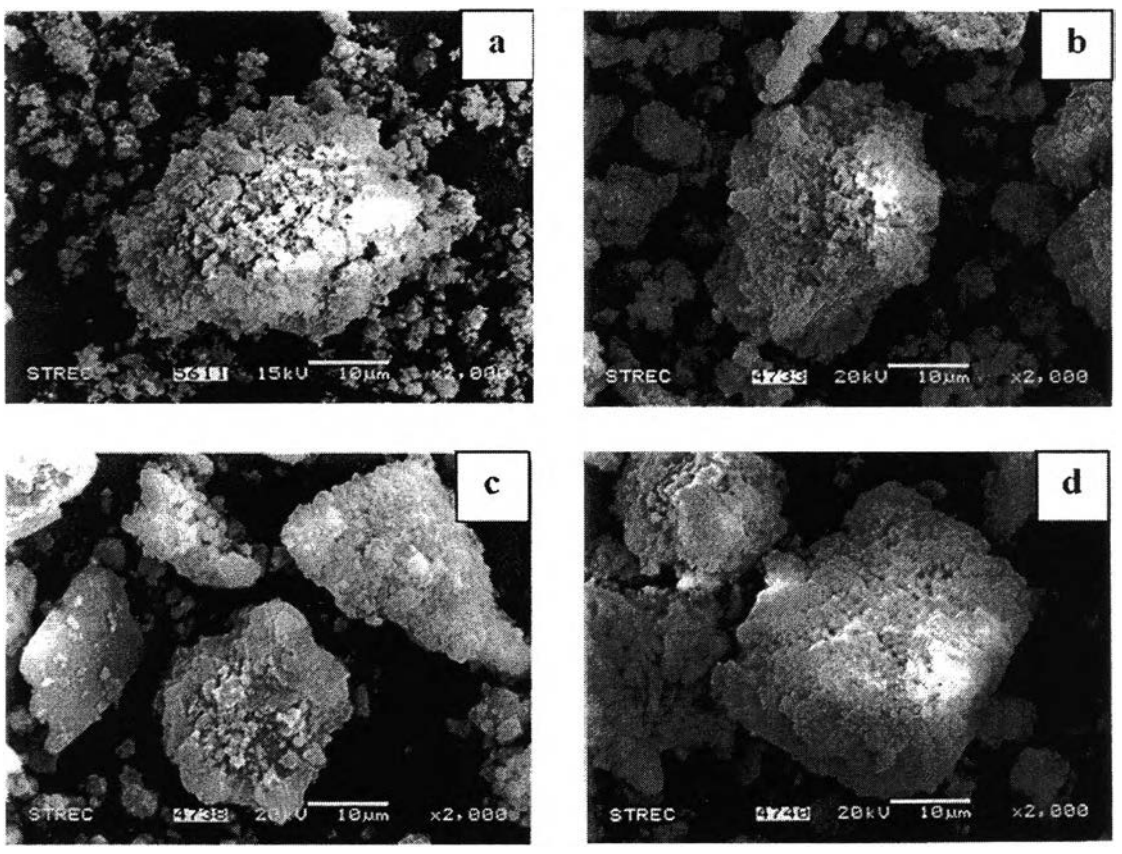

Figure 5.4 SEM micrographs of (a) 10Co/Al-10, (b) 10Co/Al-15, (c) 10Co/Al-25, and (d) 10Co/Al-35.

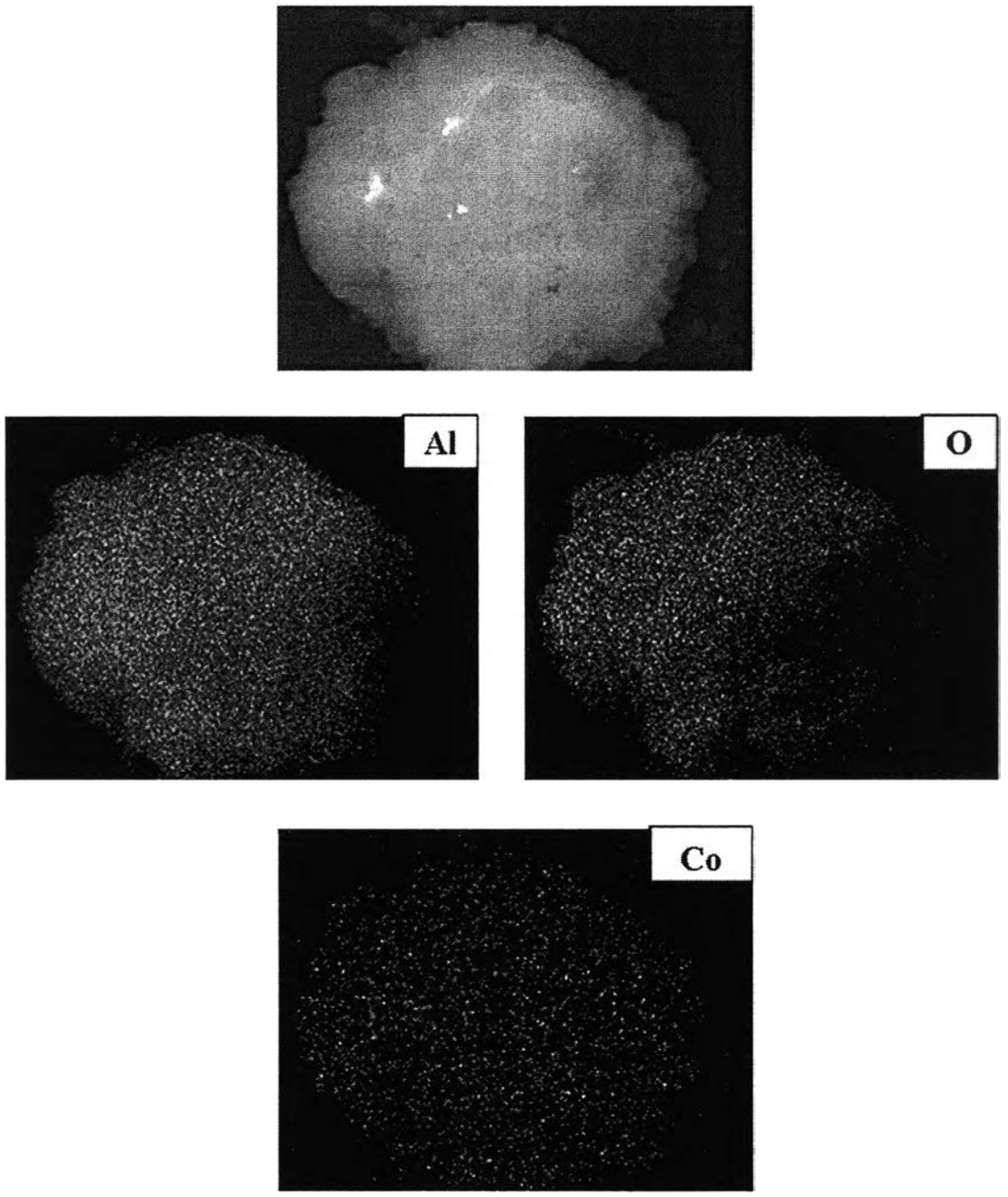

Figure 5.5 SEM micrograph and EDX mapping of cross-sectioned 10Co/Al-35 catalyst granule.

5.1.2.3 H_2 pulse chemisorption

The relative amounts of active surface cobalt on the catalyst samples were calculated from H_2 chemisorption experiments at 100°C according to Reuel and Bartholomew (Reuel and Bartholomew, 1984). It is known that only surface cobalt metal atoms are active for CO hydrogenation not its oxide or carbide (Anderson, 1984). The H_2 pulse chemisorption results are reported in Table 5.2. The amounts of H_2 chemisorption increased from 0.90 to 20.65 μmol/g cat. with increasing amount of AIP in 1-butanol used in the preparation of the alumina supports from 10 to 35 g. It is likely that the increase in the relative amounts of active cobalt metals were due to the formation of the small spherical particles of χ-alumina. As also seen in the Table 5.2, the amounts of H_2 chemisorption of 10Co/Com-Al (13.38 μmol/g cat.), prepared from the commercial γ-alumina which the crystal shape of alumina was spherical (the results was not shown), was better than solvothermal-made 10Co/γ-alumina (0.90 μmol/g cat.) but lower than 10Co/χ-alumina (20.65 μmol/g cat.). It was again confirmed that the spherical morphology of the alumina support is important in achieving the higher amount of active cobalt metal.

Table 5.2 The characteristics and H_2 chemisorption of cobalt catalyst.

Catalyst samples	Surface area (m^2/g)[a]	Amounts of H_2 chemisorption (μmol/g cat.)[a]
10Co/Al-10	61	0.90
10Co/Al-15	87	2.29
10Co/Al-25	108	7.58
10Co/Al-35	114	20.65
10Co/Com-Al*	145	13.38

[a] Error = ± 5 %, as determined directly.

* Commercial γ-alumina, BET surface area of alumina 230 m^2/g.

5.1.3 Reduction and catalytic behaviors of 10% Co/Al_2O_3 catalysts

5.1.3.1 Temperature programmed reduction (TPR)

Temperature program reduction (TPR) is a powerful tool to study the reduction behavior of the catalysts. The TPR profiles of various nanocrystalline alumina supported cobalt catalysts are shown in Figure 5.6. All the catalyst samples exhibited two main reduction peaks which could be assigned to the two-step reduction of Co_3O_4: first reduction of Co_3O_4 to CoO and then the subsequent reduction of CoO to Co^0 (Zhang *et al.*, 1999). The two reduction steps may not always be observed as separate peaks in TPR profile (Ernst *et al.*, 1999), as seen in the 10Co/Al-35 sample. A wide range of variables such as metal particle size and metal-support interaction have an influence on the reduction behavior of cobalt catalysts resulting in the observation of different locations of the TPR peaks. The TPR profiles for all the catalysts except 10Co/Al-35 appeared to be not significantly different suggesting that the AIP content had little impact on the interaction of cobalt and alumina supports. Thus, high dispersion of cobalt obtained on 10Co/Al-35 was rather to be due to the formation of small spherical particles alumina and not to the change in reducibility of the catalysts.

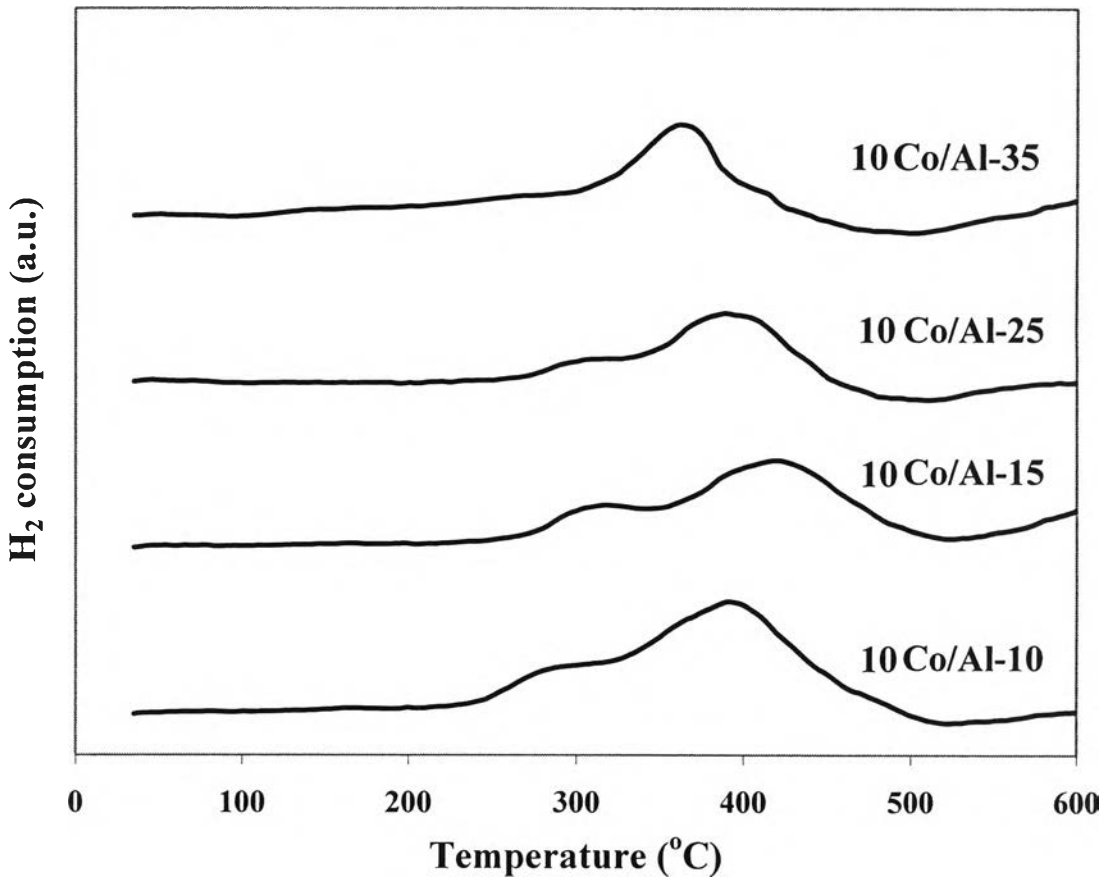

Figure 5.6 TPR profiles of the catalyst samples.

5.1.3.2 Reaction study in CO hydrogenation

CO hydrogenation reaction was carried out as a test reaction to determine the catalytic activity of the catalyst samples. The results are shown in Table 5.3. It is clearly seen that alumina prepared with higher amounts of AIP in 1-butanol resulted in much higher CO hydrogenation activities and CH_4 selectivities. The reaction results confirm the amount of surface cobalt metals measured by H_2 chemisorption.

Table 5.3 Reaction rate and selectivity for CO hydrogenation on catalyst samples.

Catalyst samples	CO conversion (%)[a]		Rate ($\times 10^2$ gCH_2 $gcat^{-1}h^{-1}$)[b]		CH_4 selectivity (%)	
	Initial[c]	SS[d]	Initial	SS	Initial	SS
10Co/Al-10	1.92	0.54	5.76	1.62	13	11
10Co/Al-15	2.63	0.75	7.89	2.25	49	47
10Co/Al-25	5.45	3.02	16.35	9.06	56	54
10Co/Al-35	8.49	4.03	25.47	12.09	70	67

[a] CO hydrogenation was carried out at 220°C, 1 atm, and H_2/CO/Ar = 80/8/32.

[b] Error ± 5%, as determined directly.

[c] After 20 min of reaction.

[d] After 6 h of reaction.

5.2 The effect of mixed γ and χ crystalline phases in Al_2O_3 on the characteristics and catalytic activities of alumina-supported cobalt catalysts during CO hydrogenation reaction

5.2.1 Characteristics of Al_2O_3 support

5.2.1.1 X-ray diffraction (XRD)

Nanocrystalline alumina powders were prepared by thermal decomposition of AIP in 1-butanol with various AIP content. XRD patterns of these alumina samples after calcination at 600°C for 1 h are shown in Figure 5.1. The XRD patterns of transition Al_2O_3 were observed at degree 2θ = 31°, 33°, 38°, 43°, 47.5°, and 68°. It was found that when lower amounts of AIP were used (10 and 15 g in 100 cm^3 of 1-butanol), only γ-Al_2O_3 was formed by calcination, as seen by the XRD characteristic peaks at 2θ = 33° according to the JCPDSs database. These γ-Al_2O_3 samples are denoted hereafter as Al-10 and Al-15, respectively. The XRD characteristic peak of χ-alumina was observed at 2θ = 42.5° for the supports prepared with higher amounts of AIP (25 and 35 g in 100 cm^3 1-butanol). The mixed γ- and χ-crystalline phase samples containing χ-phase of ca. 33% and 57% were denoted as Al-25 and Al-35, respectively. Pure χ-alumina prepared by reaction of AIP in toluene was used as the reference sample and denoted as Al-C. The intensity of χ-Al_2O_3 peaks became stronger with increasing amount of AIP content during preparation, indicating that increasing AIP content during the solvothermal synthesis resulted in formation of alumina giving rise to mixed phases of γ-Al_2O_3 and χ-Al_2O_3 after calcination.

5.2.1.2 Bulk density and BET surface area

The physical properties of the various Al_2O_3 samples are shown in Table 5.4. The BET surface area of the Al-35 (145 m^2/g) was found to be twice of that of Al-10 (70 m^2/g). A similar trend was observed for the bulk density of the Al_2O_3 powders. The bulk density increased with increasing amount of AIP used during preparation (from 0.38 g/cm^3 to 0.54 g/cm^3). The BET surface areas also increased with increasing AIP concentration, probably as a result of morphology changing from a wrinkled sheet structure to small spherical particles (see Figure 5.8). These results were confirmed by Al-C with highest BET surface area (180 m^2/g), highest bulk density (0.56 g/cm^3) and complete spherical particle morphologies. From results such as these, it has been proposed that for preparation with low AIP contents, boehmite is the main product resulting in γ-alumina after calcination at 600°C for 1 h. The morphology of the boehmite products obtained via the solvothermal reaction has been shown to be wrinkled sheets (Inoue *et al.*, 1995; Praserthdam *et al.*, 2000). The precursor to spherical-shaped χ-Al_2O_3 was formed by direct decomposition of AIP in the solvent and appeared to increase with increasing AIP concentration.

Table 5.4 Properties of the various nanocrystalline Al_2O_3 samples prepared by the reaction of AIP in 1-butanol at 300°C for 2 h.

Samples	Amounts of AIP (g)	Amounts of χ-phase (%)	Surface area (m^2/g)[a]	Bulk density (g/cm^3)[a]	Morphology
Al-10	10	-	70	0.38	Wrinkled sheets
Al-15	15	-	120	0.38	High amount of wrinkled sheets
Al-25	25	33	139	0.39	Wrinkled sheets and small amount of spherical particles
Al-35	35	57	145	0.53	Small amount of wrinkled sheets and high amount of spherical particles
*Al-C	25	100	180	0.56	Spherical particles

[a] Error of measurement = ± 5%.

* Pure χ-Al_2O_3.

5.2.1.3 Fourier transform infrared spectroscopy (FTIR)

Figure 5.7 shows the IR spectra of alumina supports after calcination at 600°C for 1 h. The IR peaks assigned to OH stretching were observed at around 3730 and broad peak between 3200 to 3600 cm^{-1}. According to Peri's model (Peri, 1965), the features at 3791, 3730, and 3678 cm^{-1} are assigned to surface isolated hydroxyl groups. The broader peak at 3589 cm^{-1} is due to the vibration of associated hydroxyl groups of aluminum oxide. The spectra which assigned to OH groups of all samples were nearly identical. Therefore, the amounts and nature of OH groups of all supports were essentially same.

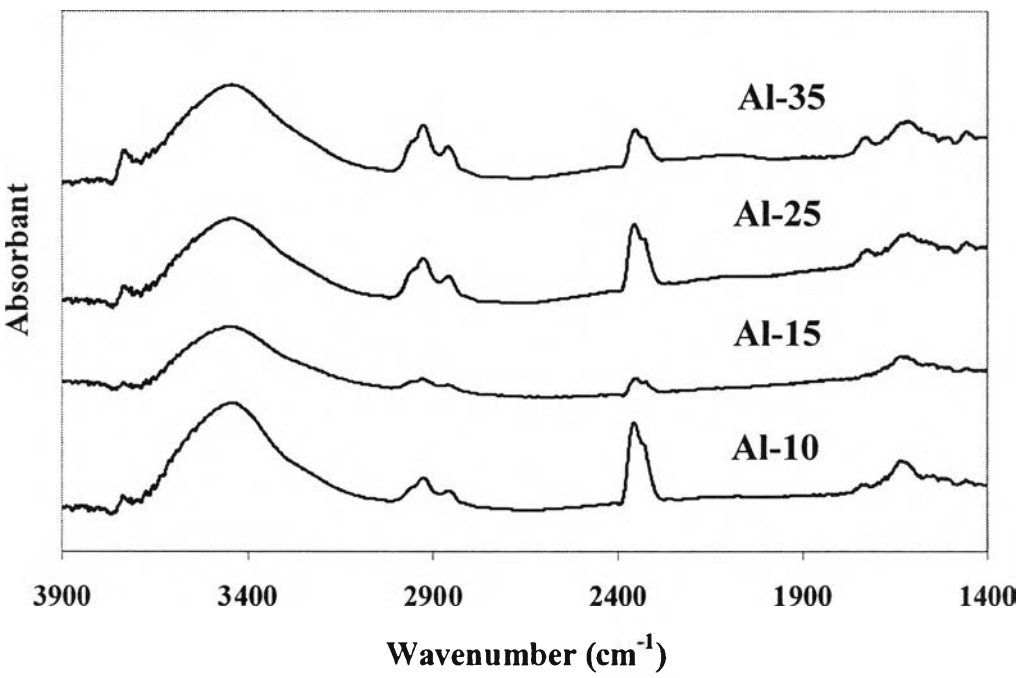

Figure 5.7 IR spectra of various alumina supports.

5.2.2 Characteristics of Co/Al_2O_3 catalysts

The nanocrystalline γ-Al_2O_3 and mixed γ- and χ-Al_2O_3 were then employed as catalyst supports for Co catalysts. The Co/Al_2O_3 catalysts were prepared using the incipient wetness impregnation method with cobalt loadings of 5, 10, 15, and 20 wt% in order to investigate the effect of mixed crystalline phases of Al_2O_3 on the dispersion of Co and its catalytic activity for CO hydrogenation.

5.2.2.1 X-ray diffraction (XRD)

The XRD patterns of the various Co/Al_2O_3 catalysts after calcination at 300°C were not significantly different from those of the Al_2O_3 supports (results not shown). No XRD characteristic peaks of Co_3O_4 and/or other Co compounds were detected for all the catalyst samples. This suggests that the crystallite size of cobalt oxide on Al_2O_3 was probably below the lower limit for XRD detectability (3-5 nm). Such results also indicate that cobalt oxide species were present in a highly dispersed form on these nanocrystalline Al_2O_3 even for cobalt loadings as high as 20 wt%.

5.2.2.2 Transmission Electron Microscopy (TEM)

The morphology and distribution of cobalt oxide particles on the Al_2O_3 supports were investigated by transmission electron microscopy (TEM). The typical TEM micrographs of 20 wt% of cobalt on alumina supports containing different compositions of γ and χ phases are shown in Figure 5.8. In all the TEM figures, the darker spots on the catalyst granules represent a high concentration of cobalt and its compounds while the lighter areas indicate the support with minimal or no cobalt present. It was found that the wrinkled sheets-like structure of γ-Al_2O_3 was maintained after impregnation and calcination for both 20Co/Al-10 and 20Co/Al-15 catalysts (Figure 5.8(a) and 5.8(b)). The mixed structure between spherical particles of χ-Al_2O_3 and wrinkled sheets of γ-Al_2O_3 were also observed for 20Co/Al-25 and 20Co/Al-35 samples (Figure 5.8(c) and 5.8(d)). However, cobalt oxide species appeared to be more agglomerated on the γ-Al_2O_3 supports than on the mixed γ- and χ-ones as shown by the appearance of larger cobalt oxide particles/granules.

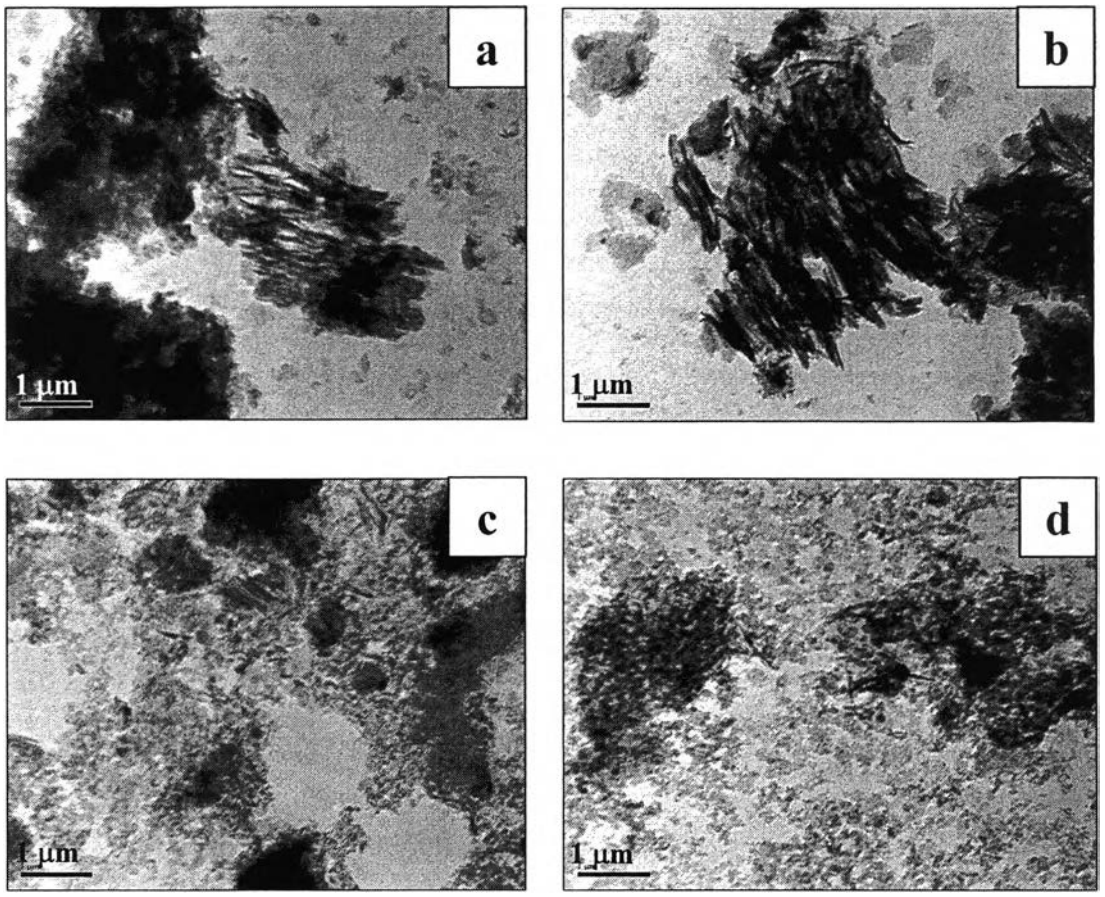

Figure 5.8 TEM micrographs of the various 20 wt% Co/Al_2O_3 catalysts (a) 20Co/Al-10 (b) 20Co/Al-15 (c) 20Co/Al-25 (d) 20Co/Al-35.

5.2.2.3 H_2 pulse chemisorption

Static H_2 chemisorption on the reduced cobalt catalyst was used to determine the number of active surface cobalt metal atoms (Jongsomjit *et al.,* 2005). The H_2 pulse chemisorption results for all catalyst samples are reported in Table 5.5. The overall dispersion of reduced Co and crystal size of Co^0 in the catalyst samples based on the H_2 chemisorption results is also given. In order to distinguish the effect of mixed γ and χ crystalline phases of Al_2O_3 and the effect of BET surface area, we also report the H_2 chemisorption results in terms of the amount of H_2 chemisorption per total specific surface area of the catalyst (see Figure 5.9). For the Co/Al-10 and Co/Al-15 catalysts in which the Al_2O_3 contained only the γ phase, the number of active surface cobalt metal atoms per unit surface area increased with increasing Co loading up to 15 wt%. Further increase of the amount of Co loading to 20 wt% resulted in both a lower cobalt dispersion and fewer exposed surface cobalt metal atoms (Table 5.5), even taking into account BET surface area (Figure 5.9). This is typical for supported Co Fischer-Tropsch catalysts. Dispersion usually decreases with increasing Co loading beyond a certain point (Backman *et al.,* 1998; Backman *et al.,* 2000; Jacobs *et al.,* 2002; Martinez *et al.,* 2003; Hosseini *et al.,* 2005). On the contrary, the amounts of H_2 chemisorption per unit surface area of the mixed γ and χ crystalline phases Al_2O_3 supported Co catalysts (Co/Al-25 and Co/Al-35) constantly increased with increasing Co loading from 5 to 20 wt% (Table 5.5, Figure 5.9). To study the effect of phase composition on active sites of Co catalyst, 15%Co/pure χ-alumina catalyst was characterized to compare with 15%Co deposited on pure γ-Al_2O_3 and mix phase supports. The amounts of H_2 chemisorption increased from 9.2 to 21.4 μmol/g catalyst as the χ phase contents increased from 0 to 57%. While the amounts of H_2 chemisorption of Co/pure χ-alumina catalyst ranged around 16.8 μmol/g catalyst. It is suggested that the presence of χ phase in γ-Al_2O_3 may prevent agglomeration of Co particles especially at high Co loadings, resulting in the maintenance of high Co dispersion.

Table 5.5 H_2 chemisorption results and ∑o Co dispersion.

Catalyst samples	Amounts of H_2 chemisorption (μmol/g cat.)[a]				% Co dispersion[b]				dp Co^0 (nm) (96.2/D%)			
	5%Co	10%Co	15%Co	20%Co	5%Co	10%Co	15%Co	20%Co	5%Co	10%Co	15%Co	20%Co
Co/Al-10	0	0.9	9.2	3.3	0	0.1	0.7	0.2	0	962	137	481
Co/Al-15	0.9	2.3	14.9	10.9	0.2	0.3	1.2	0.6	481	321	80	160
Co/Al-25	5.6	7.6	18.9	19.5	1.1	1.1	1.5	1.5	87	87	64	64
Co/Al-35	5.8	20.7	21.4	24.6	1.3	1.7	1.7	1.8	74	57	57	53
*Co/Al-C	-	-	16.8	-	-	-	1.3	-	-	-	74	-

[a] Error = ± 5 %, as determined directly.

[b] % Co dispersion = [2 × (total H_2 chemisorption/g cat.) / (no. of μmol of Co total/g cat.)] × 100 %

* Co/Al_2O_3 prepared from pure χ-Al_2O_3 support.

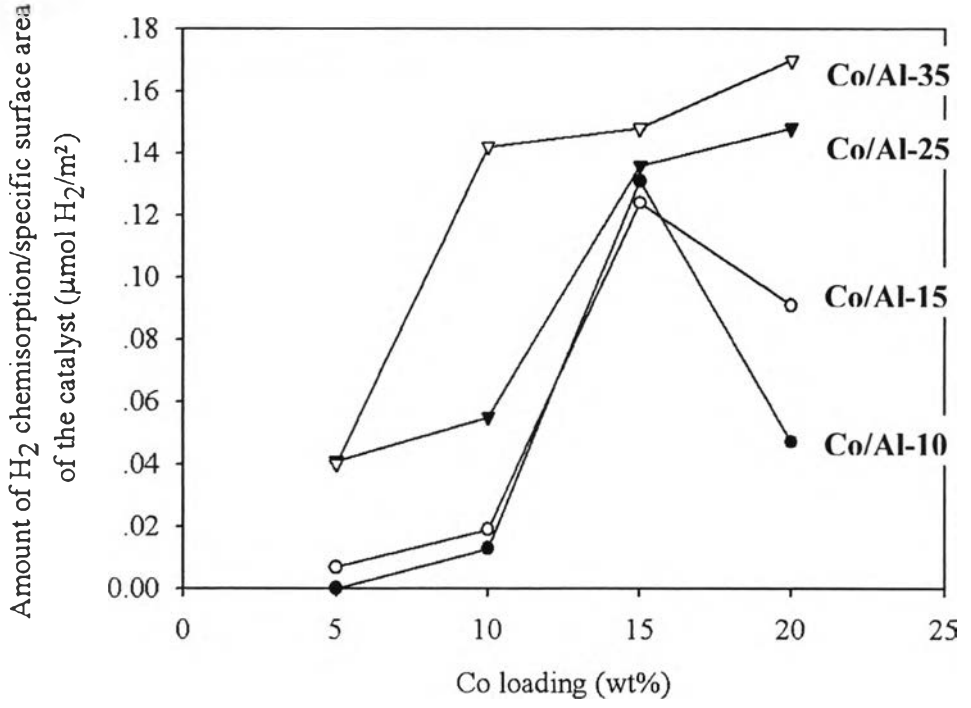

Figure 5.9 The amount of H_2 chemisorption/specific surface area of the Co/Al_2O_3 catalysts as a function of cobalt loading.

5.2.3 Catalytic behaviors of Co/Al_2O_3 catalysts

5.2.3.1 Reaction study in CO hydrogenation

CO hydrogenation was carried out in a fixed-bed quartz reactor under differential reaction conditions in order to determine the catalytic activity of the catalyst samples. The reaction results in terms of CO conversion, hydrogenation rate, and the turnover frequency (TOF) per exposed Co atom calculated using the hydrogen chemisorption data are given in Table 5.6. The catalytic activities increased with increasing Co loading in general (at least to 15 wt% Co). For a similar Co loading, Co catalysts supported on the mixed crystalline phases Al_2O_3 exhibited higher CO hydrogenation activities compared to those supported on the ones containing only γ phase Al_2O_3. The TOFs of the cobalt catalysts in which the Al_2O_3 support contained only the γ phase decreased with increasing Co loading, suggesting perhaps an underestimation of exposed Co metal atoms by H_2 chemisorption. However, the TOFs for the mixed crystalline phases Al_2O_3 did not significantly change regardless of cobalt loading percentage. The reaction results are in a good agreement with the H_2 chemisorption results since CO hydrogenation is usually considered to be a structure insensitive reaction (Ragaini *et al.*, 1996; Panpranot *et al.*, 2002; Johnson *et al.*, 1991; Iglesia, 1997; Tsubaki *et al.*, 2001). Thus, higher dispersion of Co yields higher hydrogenation activity.

Table 5.6 Reaction rate for CO hydrogenation on Co/Al_2O_3 catalysts.

Catalyst samples	CO conversion (%)[a]				Rate (μmol $gcat^{-1}s^{-1}$)[b]				TOF (s^{-1})[b,c]			
	5%Co	10%Co	15%Co	20%Co	5%Co	10%Co	15%Co	20%Co	5%Co	10%Co	15%Co	20%Co
Co/Al-10	0.5	1.9	8.8	2.1	0.3	1.1	5.2	1.3	-	0.6	0.3	0.2
Co/Al-15	1.1	2.6	10.0	4.0	0.7	1.6	6.0	2.4	0.4	0.3	0.2	0.1
Co/Al-25	2.9	5.5	10.2	7.3	1.7	3.3	6.1	4.3	0.2	0.2	0.2	0.1
Co/Al-35	4.0	8.5	10.6	10.7	2.4	5.1	6.3	6.3	0.2	0.1	0.1	0.2

[a] CO hydrogenation was carried out at 220°C, 1 atm, and $H_2/CO/Ar = 80/8/32$.

[b] Error of measurement = ± 5% as determined directly.

[c] Based on H_2 chemisorption.

5.3 The effect of Cu as an Al_2O_3-modifier on the characteristics and catalytic activities of alumina-supported iron catalysts during FTS reaction

5.3.1 Catalytic behaviors of Cu-modified Fe/Al_2O_3catalysts

5.3.1.1 Reaction study in FTS reaction

The catalytic activities and selectivities for Fischer-Tropsch synthesis of the variously Cu-modified Fe/Al_2O_3 catalysts are shown in Table 5.7. It can be seen that all the catalysts with Cu-modified Al_2O_3 supports exhibited higher hydrocarbon formation rates than the base Cu-promoted Fe/Al_2O_3 catalyst (1-0-*CC), regardless of the addition of 1% Cu as the promoter. The steady-state rates for CO_2 formation were also higher for the catalysts prepared with Cu-modified Al_2O_3 supports. For a similar catalyst system (1% Cu-promoted or non-promoted Fe/Cu-modified Al_2O_3 catalysts), the more calcination steps used during preparation, the higher the FTS activity. Hence, among the catalysts studied, the 1-10-CCC catalyst gave the highest hydrocarbon formation activity. The addition of 10% Cu on Al_2O_3 supports and/or pretreatment during preparation appear to have little effect on the FTS product selectivity, the Anderson–Schulz–Flory (ASF) chain growth probability (α), or the olefin selectivity, at least under the reaction conditions used. The results are consistent with those reported by Coville and coworkers (Coville *et al.,* 2005) that Cu promotion enhances activity of supported Fe catalysts but does not have an effect on FT product selectivity. The results from this study reveal that the effect of Cu-modified Al_2O_3 support on the catalytic properties of Fe/Al_2O_3 catalysts is similar to the addition of Cu as a second metal promoter. Moreover, the catalyst that has never been calcined in any preparation step (1-10-DDD) exhibited the lowest FTS activity among the various Fe catalysts prepared with Cu-modified Al_2O_3 supports. Therefore, the calcination step is very important in producing highly active catalysts.

Table 5.7 FTS reaction rate and selectivity.

Catalyst	Metal loading (wt%)			SS Rate of CO_2 formation [a,b] (μmol/g cat./s)	SS Rate of total HC formation [a,b] (μmol of CO converted/ g cat./s)	TOF (s^{-1})[c]	%Selectivity[b]							%Olefin (C_2-C_4)[b]	α (C_3-C_6)[b]
	Cu	Fe	Cu on Al_2O_3				C_1	C_2	C_3	C_4	C_5	C_6	C_{7+}		
1-0-*CC	1	20	0	nil	0.50	0.42	41.0	29.1	20.5	6.4	2.0	0.7	0.2	67	0.33
1-10-CCC	1	20	10	0.31	0.90	0.04	45.5	26.1	19.4	6.2	1.8	0.8	0.2	55	0.35
1-10-CDC	1	20	10	0.34	0.86	0.08	49.8	25.6	17.9	4.3	1.6	0.6	0.2	54	0.32
1-10-DDC	1	20	10	0.35	0.71	0.10	45.9	26.4	19.1	6.0	1.8	0.6	0.2	58	0.31
1-10-DDD	1	20	10	0.32	0.63	0.63	44.5	26.9	19.3	6.1	1.9	0.9	0.4	61	0.35
0-10-CC*	-	20	10	0.30	0.89	0.06	46.5	25.9	19.2	5.5	1.8	0.8	0.2	58	0.34
0-10-CD*	-	20	10	0.24	0.74	0.15	44.6	26.7	19.8	6.1	1.8	0.8	0.2	63	0.34
0-10-DC*	-	20	10	0.07[d]	0.81	0.12	43.4	27.0	20.1	6.4	2.0	0.9	0.3	58	0.35

[a] FTS reaction was carried out at 280°C, 1.8 atm total pressure, and H_2/CO ratio used = 2/1. Rate of hydrocarbon formation is in μmol of CO converted/g cat./s.

[b] Error of measurement = ± 5% as determined directly.

[c] Based on pulse CO chemisorption. Error of measurement = ± 10%.

[d] Repeatability for two times. Error of measurement = ± 2% as determined directly.

5.3.2 Characteristics of Al_2O_3 support and Al_2O_3 supported Fe catalysts

5.3.2.1 BET surface area

Some physicochemical properties of the Al_2O_3 support and the various Al_2O_3 supported Fe catalysts are shown in Table 5.8. It was found that BET surface areas, pore volumes, and pore sizes of the 1% Cu promoted Fe on the Cu-modified Al_2O_3 catalysts prepared with calcination pretreatment after the last metal impregnation (all of the 1-10 catalysts except 1-10-DDD) were in the range of 107-113 m^2/g and were not significant different from the base 1-0-*CC catalyst (115 m^2/g). On the other hand, for the 0-10 catalysts (the catalysts without 1% Cu as a second metal promoter) and the catalysts that prepared with only drying after the last metal impregnation (prior to reduction), the BET surface areas increased to 130-147 m^2/g with 0-10-CD* showed the highest BET surface area. Since the average pore sizes and pore volumes of all the catalysts were smaller than those of the alumina support, some of the active metal probably was deposited in the pores of the alumina.

Table 5.8 Some properties of the catalysts.

Catalyst	Metal loading (wt%)			BET surface area (m^2/g cat.)[a]	Avg. Pore Vol. (cm^3/g cat.)[a]	Avg. Pore size (nm)[a]	CO chemisorption (μmol/g cat.)[b]
	Cu	Fe	Cu on Al_2O_3				
γ-Al_2O_3	0	0	0	100.0	0.68	27.2	-
1-0-*CC	1	20	0	114.8	0.37	12.9	1.2
1-10-CCC	1	20	10	107.4	0.36	13.4	24.8
1-10-CDC	1	20	10	113.1	0.35	12.5	11.2
1-10-DDC	1	20	10	108.6	0.35	12.9	6.9
1-10-DDD	1	20	10	145.7	0.35	9.7	1.0
0-10-CC*	0	20	10	130.4	0.36	11.0	15.2
0-10-CD*	0	20	10	146.7	0.32	8.8	4.8
0-10-DC*	0	20	10	130.4	0.35	10.8	6.8

[a] Using N_2 physisorption at 77 K. Error of measurement = ± 10%

[b] Error of measurement = ± 5%.

5.3.2.2 X-ray diffraction (XRD)

XRD patterns of the Al_2O_3, the calcined 10 wt% Cu/Al_2O_3, and the catalyst samples are shown in Figure 5.10. According to the JCPDS database, the γ-Al_2O_3 exhibited strong diffraction peaks at $2\theta = 31^o$, 33^o, 38^o, 39.7^o, 43^o, 46^o, and 68^o. For the 10% Cu/Al_2O_3 catalyst, it was found that Cu was in the form of CuO as indicated by their characteristic peaks at $2\theta = 35.5^o$ and 39^o. It has been reported that interaction between CuO and Al_2O_3 occurs readily at calcination temperatures close to 600°C, yielding $CuAl_2O_4$ (El-Shobaky *et al.,* 1999). Moreover, the extent of solid–solid interaction between oxides involved in the aluminate formation increases on increasing the calcination temperature from 600 to 800°C. It is likely that in this study $CuAl_2O_4$ was not formed at the calcination temperature used (460°C) since no XRD peaks for of $CuAl_2O_4$ were detected. The XRD patterns for all the supported Fe catalysts do not show any characteristic peaks of Fe_2O_3 or any other Fe compounds suggesting that Fe was present in a highly dispersed form. Except for the catalysts that were only dried after the last metal impregnation, all the catalysts exhibited XRD patterns similar to the base catalyst where only the major peaks for γ-Al_2O_3 were found. For the 1-10-DDD and 0-10-CD* catalysts which were only dried after the last metal impregnation, additional diffraction peaks at $2\theta = 12.9^o$, 20.9^o, and 25.8^o can be seen in the XRD patterns. These peaks were attributed to the presence of residual Fe nitrate of Cu nitrate in the catalysts which resulted in hard to reduce Fe oxide to Fe metal when reduction the catalysts with H_2 were carried out. Hence these catalysts were less active than those prepared with calcination pretreatment after impregnation of metals.

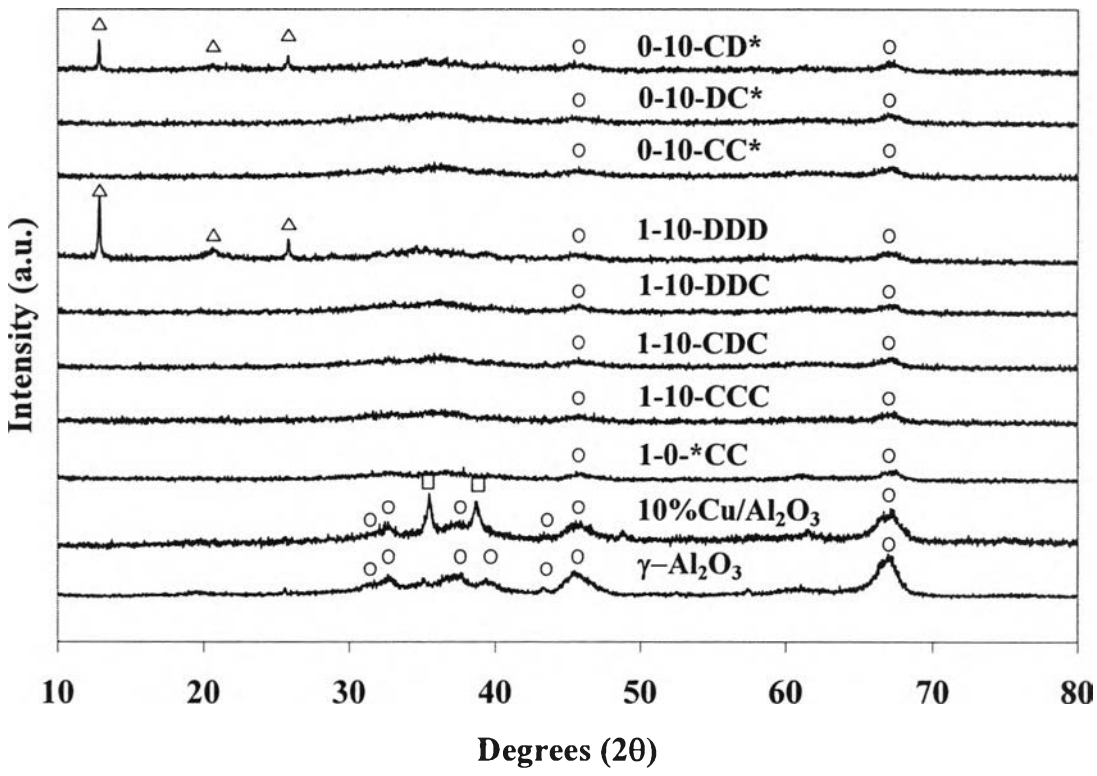

Figure 5.10 XRD patterns of Al_2O_3 supported Fe catalyst and Cu-modified Al_2O_3 supported Fe catalyst. ○ - γ Al_2O_3; □ - CuO; △ - Nitrate species

5.3.2.3 Electron microscopy

SEM and EDX were also performed in order to study the morphology and elemental distribution of the catalyst samples. Figure 5.11 shows the typical SEM micrographs of the external surface of γ-Al_2O_3 (Figure 5.11(a)) and Cu-modified alumina supports (Figure 5.11(b)). It can be observed that alumina support consisted of irregular shape particles/granules formed by agglomeration of nanocrystalline alumina. Loading of 10% Cu on the alumina supports resulted in the same irregular shape particle/granules. There were no differences in the cluster size and morphology of the variously 20% Fe/Al_2O_3 catalysts as seen in Figure 5.12. Figure 5.13 shows an SEM micrograph along with the elemental mapping (for Al, O, Fe, and Cu) of the 1-10-CCC catalyst. It can be seen that all of elements in the catalyst were well dispersed and distributed throughout the catalyst granules. Similar results were also obtained for other Cu-modified alumina supported Fe catalysts.

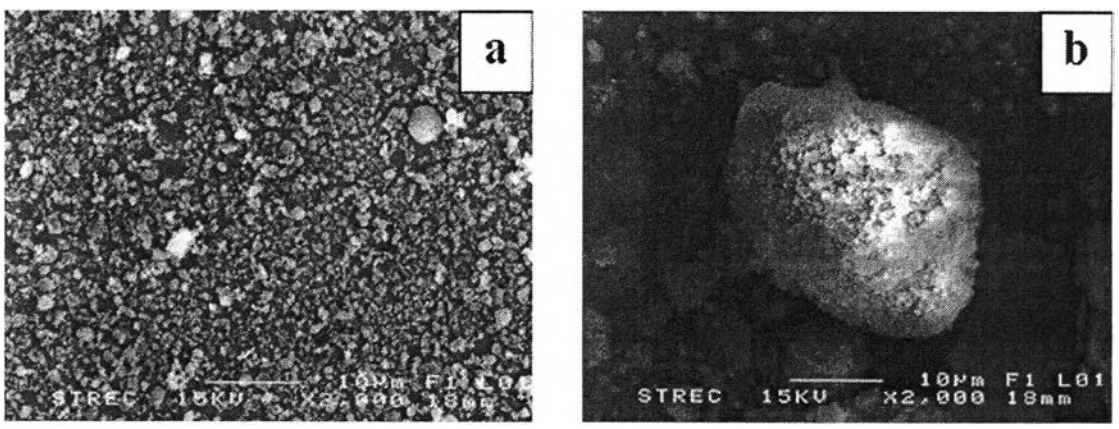

Figure 5.11 SEM micrographs of (a) γ-Al_2O_3, (b) Cu-modified Al_2O_3.

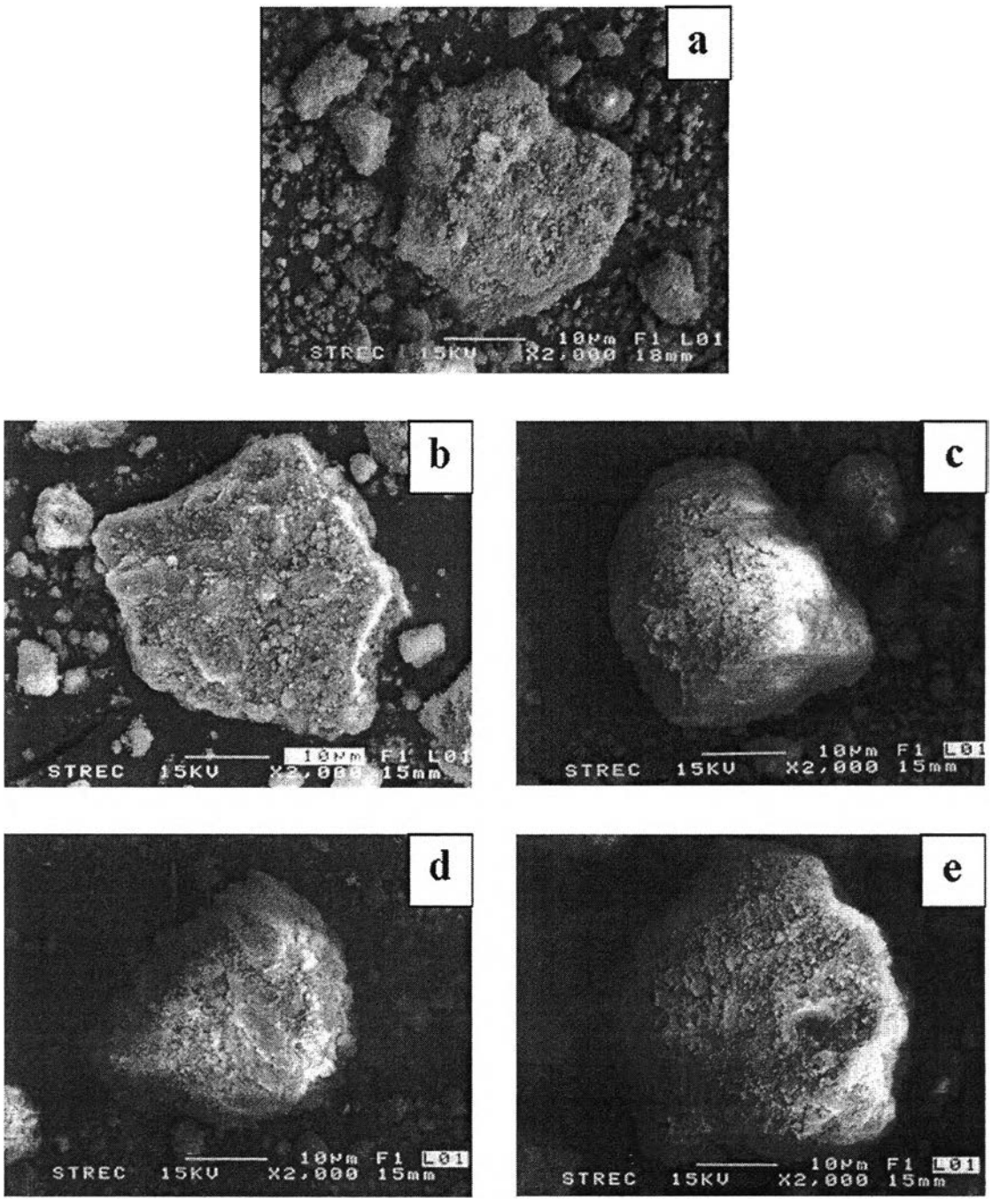

Figure 5.12 SEM micrographs of the catalysts. (a) 1-0-*CC, (b) 1-10-CCC, (c) 1-10-DDC, (d) 1-10-DDD and (e) 0-10-CC*

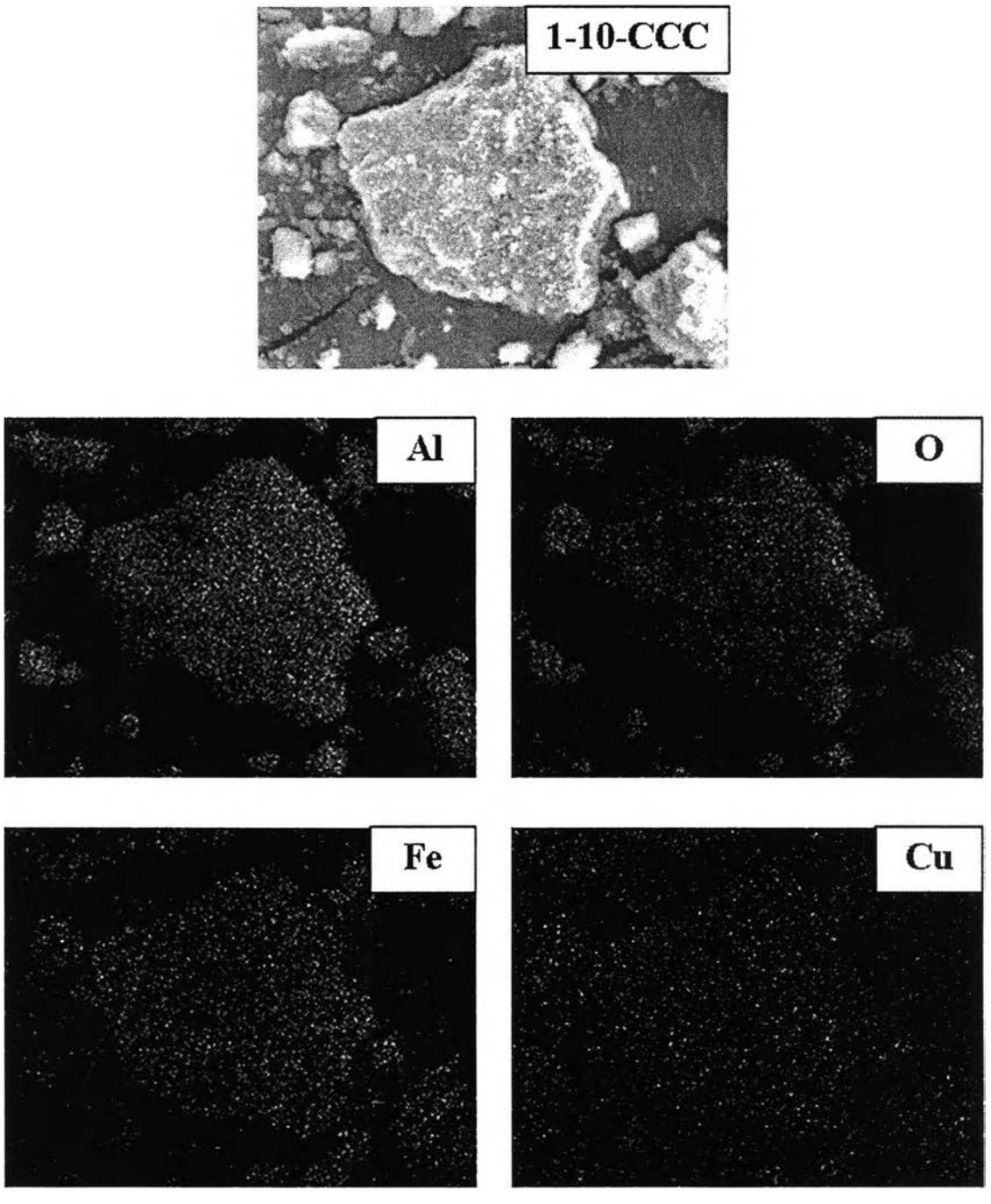

Figure 5.13 SEM micrograph and EDX mapping of cross-sectioned 1-10-CCC catalyst granule.

5.3.2.4 Temperature programmed reduction (TPR)

Temperature program reduction (TPR) is a powerful tool to study the reduction behavior of the catalysts. The TPR profiles of the Fe/Al_2O_3 catalyst and the variously Cu-modified Fe/Al_2O_3 catalysts are shown in Figure 5.14. TPR profile of alumina support (not shown) exhibited no reduction peak at this TPR condition. It was found that TPR profile of the Fe/Al_2O_3 catalyst (0-0-*C*) shown reduction peak at ca. 220-470°C (max. at 393°C). For 1%Cu-promoted Fe/Al_2O_3 catalyst, only one reduction peak located at ca. 165-400°C (max. at 265°C) can be observed. TPR profiles for the Cu-modified Fe/Al_2O_3 catalysts were also similar exhibiting only one reduction peak. The reduction peak of the Cu-modified Fe/Al_2O_3 catalysts (except 1-10-DDD and 0-10-CD*) were located at ca. 105-345°C (max. at 230°C). While, the reduction peak of the 1-10-DDD and 0-10-CD* catalysts were located at ca. 200-400°C (max. at 330°C). The maximum temperature at ca. 265°C for the 1%Cu-promoted Fe/Al_2O_3 catalyst was shifted about 35°C when there was a presence of Cu modifier in the alumina support as seen for the Cu-modified Fe/Al_2O_3 catalysts (except 1-10-DDD and 0-10-CD*). The shift of a reduction peak to a lower temperature indicates weaker interaction between iron and alumina support. For the Cu-modified Fe/Al_2O_3 catalysts using dry pretreatment after the final impregnation (1-10-DDD and 0-10-CD*), the maximum temperature at ca. 265°C for the 1%Cu-promoted Fe/Al_2O_3 catalyst was shifted about 65°C. The shift of a reduction peak to a higher temperature indicates stronger interaction between iron and alumina support. It was suggested that the presence of the Cu-modification on the alumina supported iron catalysts using dry and calcination pretreatment after the final impregnation decreased the reduction temperature of the catalysts. However, the one using only dry pretreatment after the final impregnation resulted in increasing the reduction temperature. This should be due to the presence of residual nitrate species in the catalysts which resulted in hard to reduce Fe oxide to Fe metal.

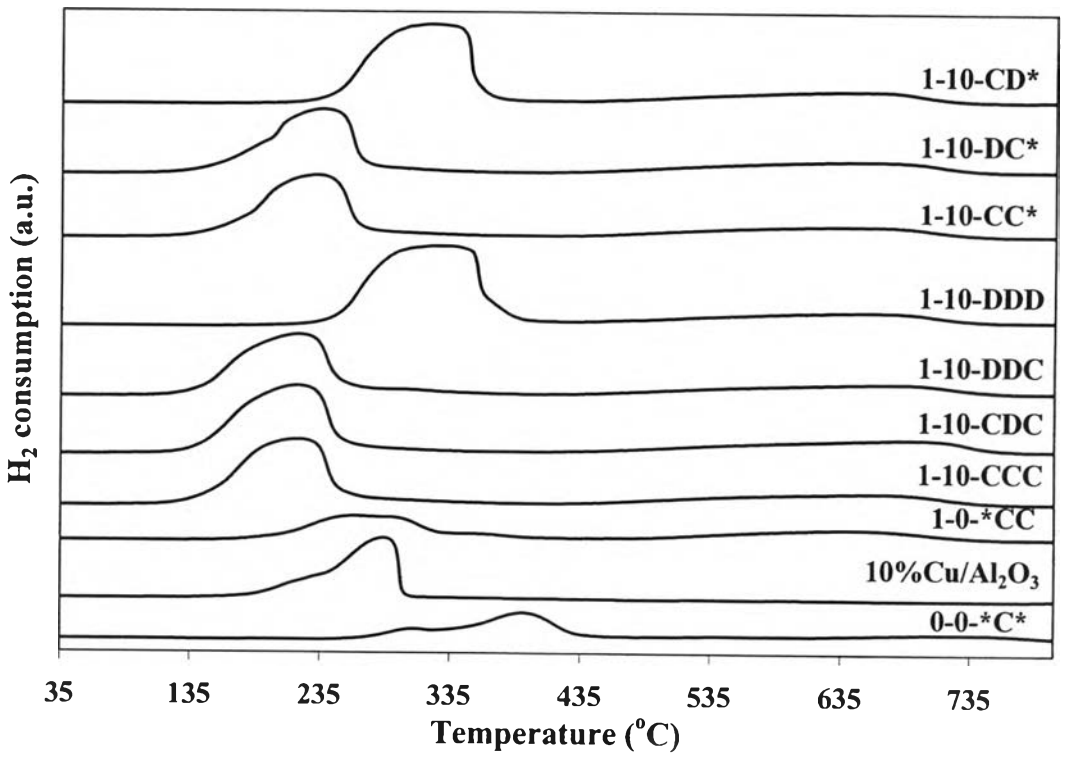

Figure 5.14 TPR profiles of the catalyst samples.

0-0-*C* referred to 20% Fe/Al_2O_3 catalyst.

5.3.2.5 CO pulse chemisorption

Pulse CO chemisorption was performed to determine the relative amounts of active iron surface atoms on the catalyst samples. The results are also shown in Table 5.8. It can be seen that the amounts of CO chemisorption of Cu-modified Fe/Al_2O_3 catalysts were in the range of 1.0-24.8 μmol/gcat. and were higher than Fe/Al_2O_3 catalysts. It is likely that the presence of the Cu in the alumina support resulted in the increase in the relative amounts of active iron metals. Pulse CO chemistorption is difficult on Fe often. However, the CO chemisorption results are very useful. It can be seen in Figure 5.15 that, for the Cu-modified Fe/Al_2O_3 catalysts, each additional calcination seemed to lead to increased CO chemisorption. Figure 5.16 shows the effect of the number of calcinations on the steady state of hydrocarbon rate. It was found that there was a significant increase in the steady state of hydrocarbon rate with the number of calcinations. Considering the effect of the number of calcinations on the rate of CO_2 formation in Figure 5.17, it can be seen that there was less (or no) effect on the rate of CO_2 formation, although the Cu modification significantly increased water- gas-shift reaction on the catalysts. Figure 5.18 shows the plot between steady state of total hydrocarbon rate and CO chemisorption. It can be observed that there was an increase in the rate with increased in CO chemisorption, but there was only a weak dependence (increased in a factor of 25 only resulted in an increase in the rate of ca. 50%). From the results above, it would appear that the important variable besides Cu-modification of the support is the number of calcinations. It is known that CO chemisorption does not necessarily relate directly to the number of active sites. Perhaps multiple calcinations (a) decrease the contamination of the surface by nitrate species, (b) increase Fe reducibility, and/or (c) produce large Fe particles.

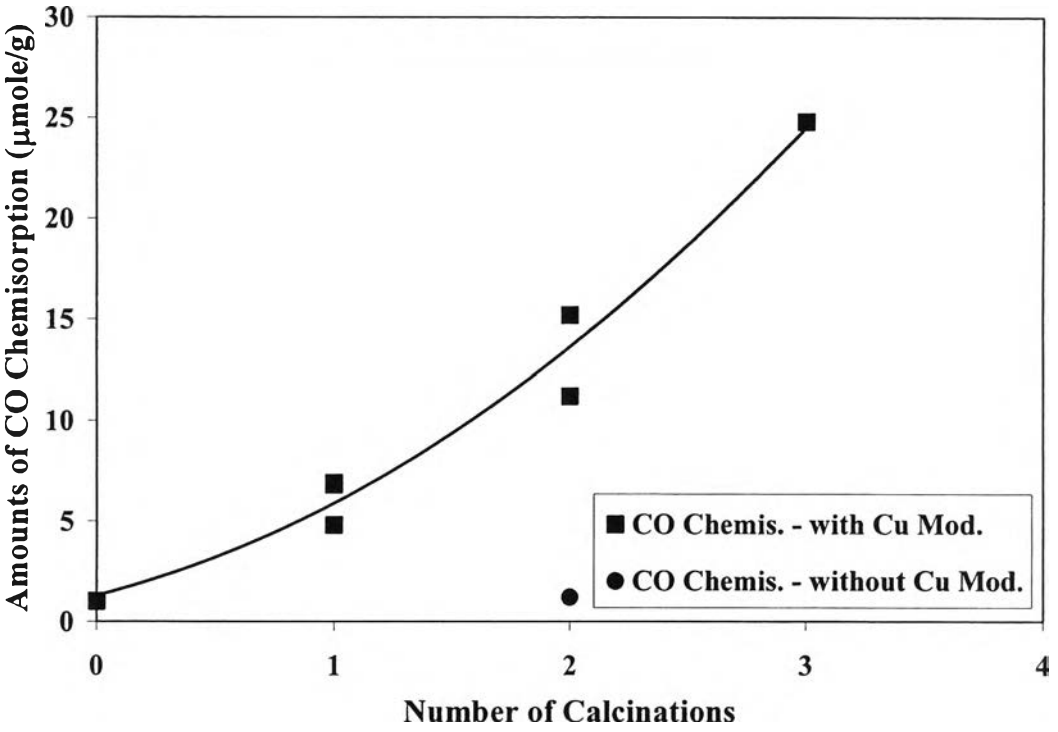

Figure 5.15 Effect of number of calcinations on CO chemisorption.

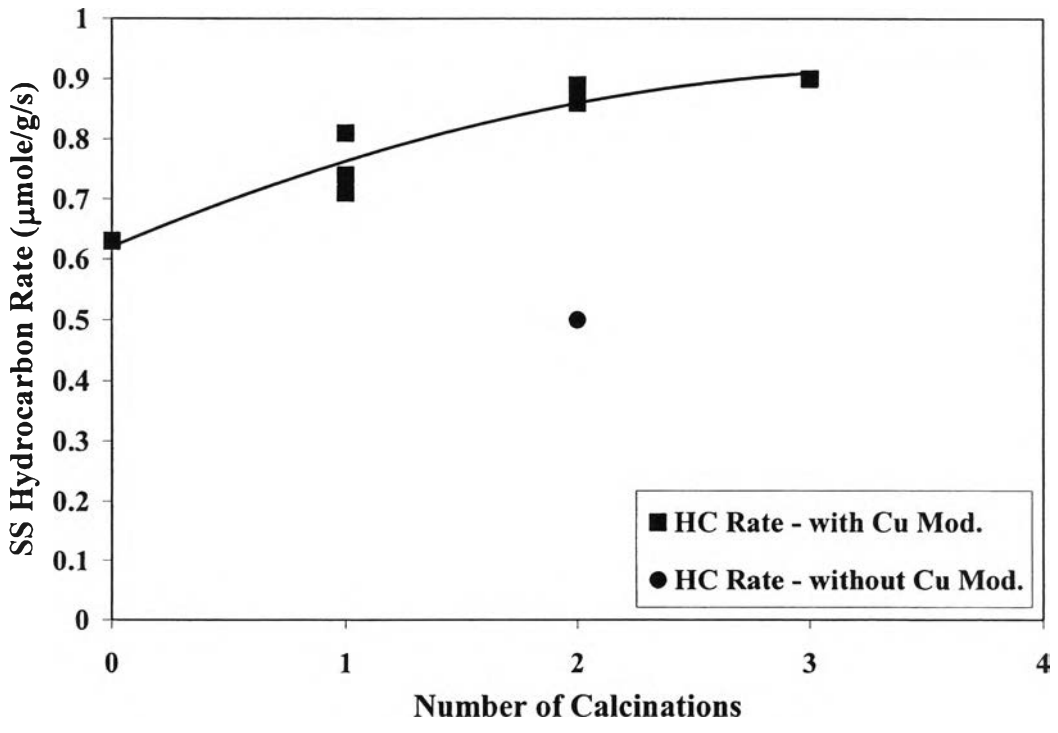

Figure 5.16 Effect of number of calcinations on steady state of total hydrocarbon rate.

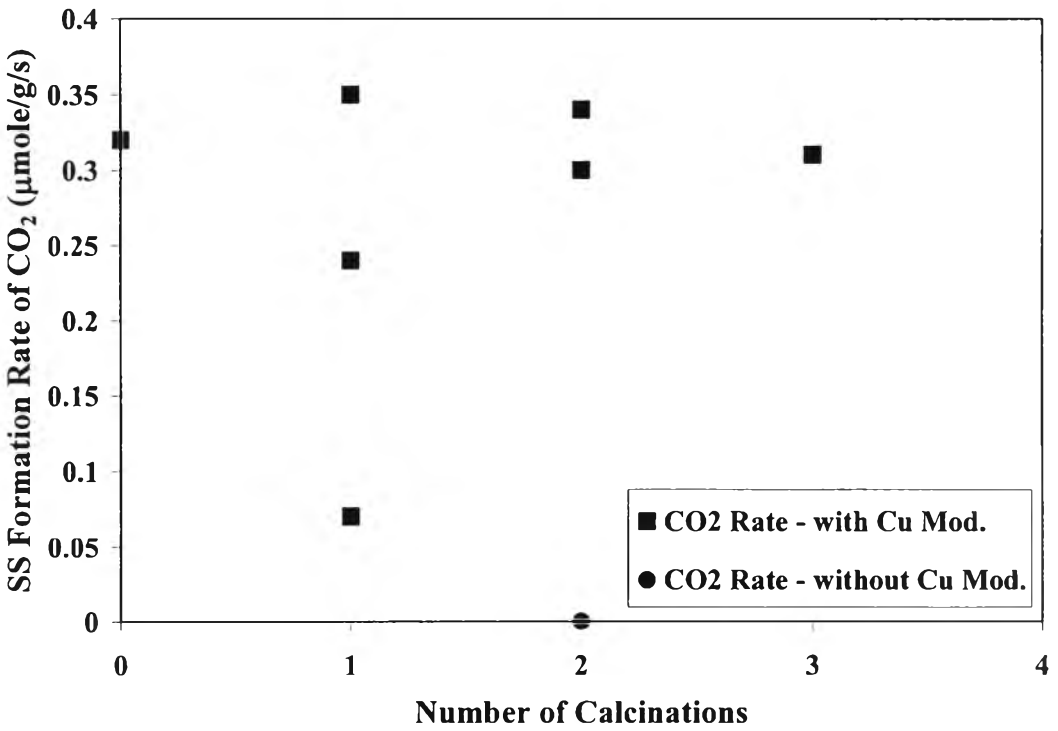

Figure 5.17 Effect of number of calcinations on steady state formation rate of CO_2.

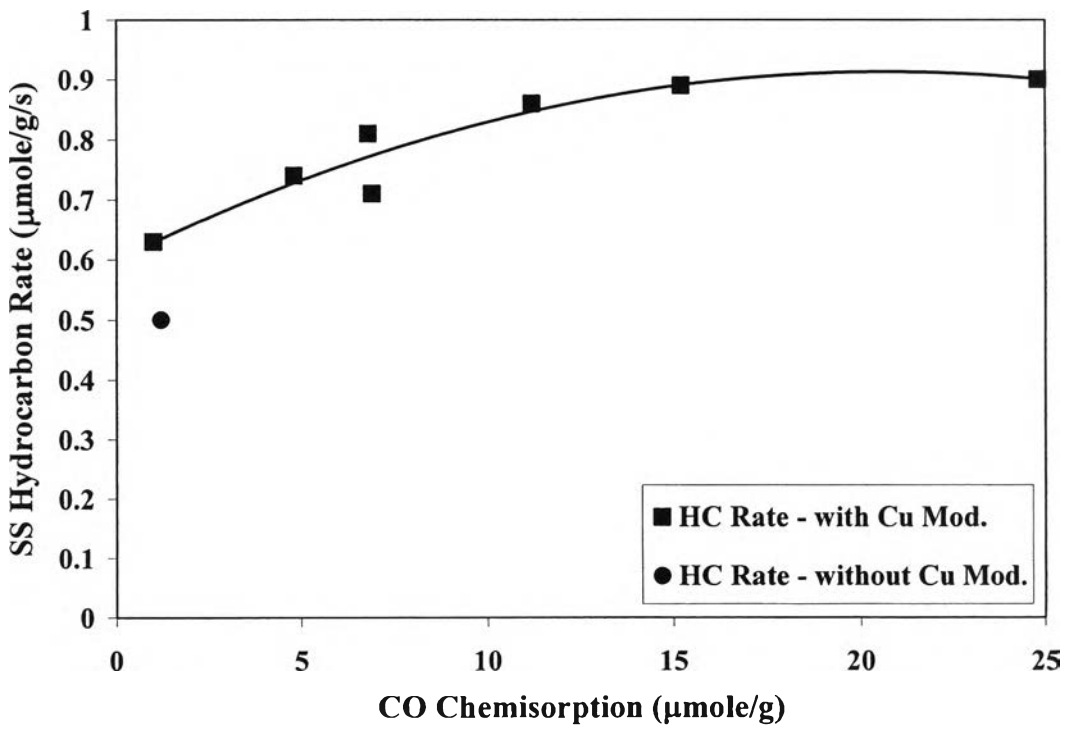

Figure 5.18 Steady state of total hydrocarbon rate vs. CO chemisorption.